Available online at www.sciencedirect.com
SCIENCE DIRECT®
International Journal of Thermal Sciences 44 (2005) 799–807
International Journal of Thermal Sciences
www.elsevier.com/locate/ijts

Finned tube banks configuration for the utilization of waste heat from a gas turbine station

Guyh Dituba Ngoma [a,*], Amsini Sadiki [b]

[a] *Department of Applied Sciences, University of Quebec in Abitibi-Temiscamingue, 445, Boulevard de l'Université, Rouyn-Noranda, Quebec, J9X 5E4, Canada*
[b] *Department of Energy and Power Plant Technology, Darmstadt University of Technology, Petersenstrasse 30, 64287 Darmstadt, Germany*

Received 14 April 2004; received in revised form 21 January 2005; accepted 24 January 2005
Available online 7 April 2005

Abstract

In this work, a computational model was developed to predict and analyze static behavior in two different systems of dual-pressure finned tube banks to be used behind a gas turbine station without a pre-existing heat recovery system. The relevant physical phenomena were accounted for by means of a non-linear approach and the difference between water and steam velocities in finned tubes. Simulations were also done considering the effects of exhaust gas parameters and tube length on the flow-fields of the working fluid. The results revealed the different static performance of these models on the sides of the working fluid and exhaust gas.

Keywords: Finned tube banks; Two-phase flow; Power system; Combined-cycle; Modeling and simulation

1. Introduction

Due to of the recent global trends to deregulate the energy market and reduce environmental pollution, heat flow exchangers are commonly installed behind existing gas turbine stations, e.g. a gas turbine for a compressor station [1–3]. This allows recovery of the waste heat found in the hot exhaust gas from a gas turbine. There are many different flow arrangements that can be used for the heat transfer between the working fluid and the exhaust gas from a gas turbine with a heat recovery system. Here, the working fluid flows through the finned tube banks and the exhaust gas passes across them. The steam produced is used to power a steam turbine, which drives an electric generator. This enhances overall system efficiency [4]. The arrangement of the tube banks depends on the available space behind the gas turbine. Dual-pressure systems use both parallel and serial configurations for the gas tube banks. In the parallel flow tube banks, the exhaust gas heats water flows at each pressure at the same time. In the serial configuration, the exhaust gas sequentially heats the tube banks [4–6]. Since these tube banks are very compact, their configuration is important for system performance, including the optimal utilization of the exhaust gas and the reliability and safety of power plant operations. An investigation of system performance as part of the planning and design of a power plant improves both static and dynamic operating phase system behavior. Most previous investigations of exhaust gas flow across tube banks were performed considering a homogeneous equilibrium model for a two-phase flow on the tube side [7–9]. The homogeneous equilibrium model assumes that the steam and water phases are flowing at the same velocity. Additionally, analysis of previous works reveals that the effect in change in exhaust gas temperature across finned tube banks is neglected, and the results are specific for the tube banks configuration and therefore cannot be extrapolated to other configurations. In this work, a computational model is developed to allow for selection of the appropriate distribution of heating surfaces for connection to a gas turbine without a pre-existing heat recovery system in order to maximize the efficiency and

* Corresponding author.
E-mail address: guyh.dituba-ngoma@uqat.ca (G.D. Ngoma).

1290-0729/$ – see front matter
doi:10.1016/j.ijthermalsci.2005.01.008

Nomenclature

A	tube cross sectional area	m^2
C_0	distribution factor	
c	specific heat	$J{\cdot}kg^{-1}{\cdot}K^{-1}$
d	diameter	m
Fr	Froude number	
g	acceleration due to gravity	$m{\cdot}s^{-2}$
h	specific enthalpy	$J{\cdot}kg^{-1}$
$\dot{m}$	mass flow rate	$kg{\cdot}s^{-1}$
p	pressure	Pa
Pr	Prandtl number	
$\dot{q}$	heat flux	$W{\cdot}m^{-2}$
Re	Reynolds number	
r	vaporization heat	$J{\cdot}kg^{-1}$
t	time	s
U	tube circumference	m
u	internal energy	$J{\cdot}kg^{-1}$
V_{Gj}	drift velocity	$m{\cdot}s^{-1}$
We	Weber number	
w	flow velocity	$m{\cdot}s^{-1}$
$\dot{x}$	steam quality	
z	axial coordinate	m

Greek symbols

α	convection heat transfer coefficient	$W{\cdot}m^{-2}{\cdot}K$
β	tube orientation angle from the horizontal	°
Δ	difference of a variable	
ε	void fraction	
ε_r	absolute roughness	m
η	dynamic viscosity	Pa·s
λ	thermal conductivity	$W{\cdot}m^{-1}{\cdot}K^{-1}$
ϑ	temperature	°C
ρ	density	$kg{\cdot}m^{-3}$
σ	surface tension	$N{\cdot}m^{-1}$
ξ	friction factor	

Subscripts

i	inner
G	steam phase
L	water phase
o	outer
R	friction pressure drop
sat	saturation
w	tube wall
wf	working fluid
hg	hot exhaust gas

economic benefits of the entire plant. Here, we consider the concept of the dual-pressure levels on the operating fluid [4,5]. Two different configurations of tube banks systems were numerically analyzed. Non-linear mathematical systems of equations of mass, momentum and energy were developed in the modeling process. A two-phase steam-water flow was simulated using the drift flux model according to Rouhani's correlation, which takes into account the velocities of water and steam phases [10,11]. The influence of the tube length and tube walls on the system's thermal performance was included. The effects of exhaust gas parameters on the flow-fields of the working fluid were also investigated and analyzed.

2. Model description

Figs. 1 and 2 show the two examined models, which consist of dual-pressure once-through heat recovery steam generator (HRSG) systems in cross flow with finned tube banks

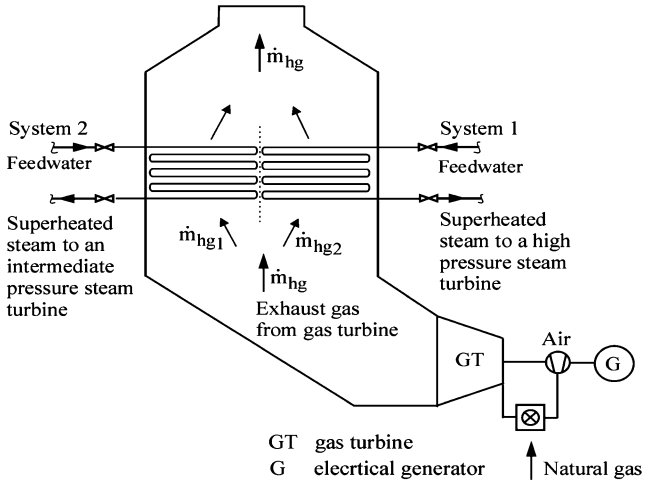

Fig. 1. Dual pressure once-through HRSG systems in parallel configuration.

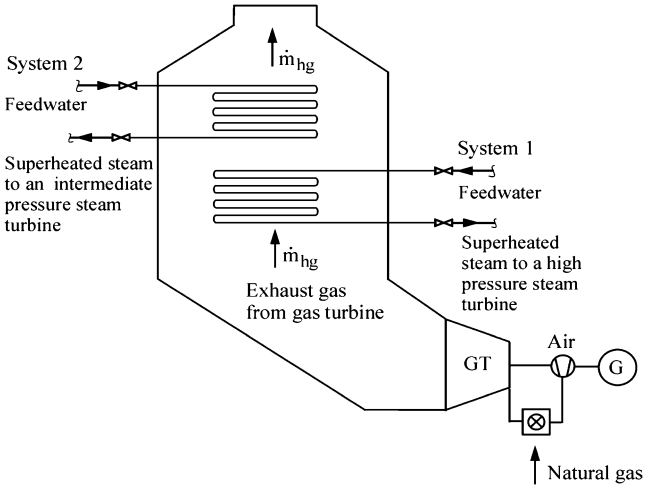

Fig. 2. Dual pressure once-through HRSG systems in serial configuration.

and a gas turbine with a vertical outlet for the exhaust gas. Model 1 uses a parallel configuration and is characterized by 50% of the total exhaust gas flow rate for the systems 1 and 2, i.e.

$$\dot{m}_{\mathrm{hg1}} = \dot{m}_{\mathrm{hg2}} = \frac{\dot{m}_{\mathrm{hg}}}{2}$$

Model 2 uses a serial configuration. Both models have the same geometry.

3. Governing equations

To develop the governing equations for the considered models, the following assumptions were made:

(a) A steady state, one-dimensional flow was assumed.
(b) A constant tube cross section was assumed.
(c) The two-phase flow was considered to be a mixed model of water and steam, i.e. the water and steam pressures were the same on the two-phase interface.

To account for these assumptions, the theoretical analysis of a tube of the once-through HRSG systems shown in Figs. 1 and 2 is based on the conservation equations of mass, momentum and energy for exhaust gas (single-phase flow), working fluid (single-phase and two-phase flow) and tube wall [12–15]. For a single-phase flow, mass conservation is given by:

$$\frac{\partial(\rho w A)}{A\partial z} = 0 \tag{1}$$

where A, w, z and ρ are the tube cross section, flow velocity, axial coordinate and density, respectively. Eq. (1) leads to the following expression of the mass flow rate:

$$\dot{m} = \rho w A = \text{constant} \tag{2}$$

For the two-phase flow, it can be written as follows:

$$\frac{\partial}{A\partial z}\big(\rho_L(1-\varepsilon)w_L + \rho_G\varepsilon w_G\big)A = 0 \tag{3}$$

The mixture mass flow rate can be expressed by

$$\dot{m} = \big(\rho_L(1-\varepsilon)w_L + \rho_G\varepsilon w_G\big)A \tag{4}$$

where the water phase velocity is given by

$$w_L = \frac{(1-\dot{x})\dot{m}}{(1-\varepsilon)\rho_L A} \tag{5}$$

and the steam phase velocity follows as

$$w_G = \frac{\dot{x}\dot{m}}{\varepsilon\rho_G A} \tag{6}$$

The other symbols and subscripts used were defined in the nomenclature.

In the two-phase flow, the difference between water and steam phase velocities ($w_G - w_L$) was taken into consideration by means of the Rouhani correlation [10], which is valid for a two-phase flow in horizontal and vertical tubes, and for the steam quality between 0 and 1. The void fraction according to Rouhani is formulated as follows:

$$\varepsilon = \frac{\dot{x}/\rho_G}{C_0[\dot{x}/\rho_G + (1-\dot{x})/\rho_L] + AV_{Gj}/\dot{m}} \tag{7}$$

where

$$A = \frac{\pi d_i^2}{4} \tag{8}$$

$$C_0 = 1 + 0.12(1-\dot{x}) \tag{9}$$

$$V_{Gj} = V_{Gj}^*\left[\frac{\sigma_L g(\rho_L - \rho_G)}{\rho_L^2}\right]^{0.25} \tag{10}$$

$$V_{Gj}^* = 1.18(1-\dot{x}) \tag{11}$$

The momentum equation for a single-phase flow is defined by

$$0 = \frac{\partial(\rho w^2)}{\partial z} + \rho g\sin\beta + \frac{\partial p}{\partial z} + \left|\frac{\partial p}{\partial z}\right|_R \tag{12}$$

Since density depends on pressure and temperature, $\rho = \rho(p,\vartheta)$, in a single-phase flow, the partial differential of the density in the z direction can be written as

$$\frac{\partial\rho}{\partial z} = \frac{\partial\rho}{\partial p}\frac{\partial p}{\partial z} + \frac{\partial\rho}{\partial\vartheta}\frac{\partial\vartheta}{\partial z} \tag{13}$$

By taking into account Eq. (13), the partial differential of the pressure in z direction can be expressed as

$$\frac{\partial p}{\partial z} = \frac{C_{s1}}{C_{s2}} \tag{14}$$

with

$$C_{s1} = -\frac{1}{A}Y_{s1} - \rho g\sin\beta - \left|\frac{\partial p}{\partial z}\right|_R \tag{15}$$

$$Y_{s1} = 2w\frac{\partial\dot{m}}{\partial z} - \frac{\dot{m}^2}{A\rho^2}\frac{\partial\rho}{\partial\vartheta}\frac{\partial\vartheta}{\partial z} \tag{16}$$

$$C_{s2} = 1 - \frac{\dot{m}^2}{A^2\rho^2}\frac{\partial\rho}{\partial p} \tag{17}$$

and for a two-phase flow, it can be given by

$$\frac{\partial}{\partial z}\big(\rho_L(1-\varepsilon)w_L^2 + \rho_G\varepsilon w_G^2 + p\big) + \big(\rho_L(1-\varepsilon) + \rho_G\varepsilon\big)g\sin\beta + \left|\frac{\partial p}{\partial z}\right|_R = 0 \tag{18}$$

Since the density in a two-phase flow depends on the pressure, $\rho_k = \rho_k(p)$ with $k = L, G$, the partial differential of the density in z direction can be formulated as

$$\frac{\partial\rho_k}{\partial z} = \frac{\partial\rho_k}{\partial p}\frac{\partial p}{\partial z} \tag{19}$$

The void fraction depends on pressure and steam quality:

$$\varepsilon = \varepsilon(p,\dot{x}) \tag{20}$$

Eq. (20) leads to the following partial differential of the void fraction in z direction:

$$\frac{\partial \varepsilon}{\partial z} = \frac{\partial \varepsilon}{\partial p}\frac{\partial p}{\partial z} + \frac{\partial \varepsilon}{\partial \dot{x}}\frac{\partial \dot{x}}{\partial z} \tag{21}$$

The partial differential of the pressure in the z direction can be written with Eqs. (19)–(21) as

$$\frac{\partial p}{\partial z} = \frac{C_{t1}}{C_{t2}} \tag{22}$$

with

$$C_{t1} = -\left(E_1\frac{\partial \varepsilon}{\partial \dot{x}} + 2\frac{\dot{m}}{A}(-w_L + w_G)\right)\frac{\partial \dot{x}}{\partial z} - Y_{t1} \tag{23}$$

$$E_1 = \rho_L w_L^2 - \rho_G w_G^2 \tag{24}$$

$$Y_{t1} = \big(\rho_L(1-\varepsilon) + \rho_G\varepsilon\big)gsn\beta + \left|\frac{\partial p}{\partial z}\right|_R \tag{25}$$

$$C_{t2} = 1 - (1-\varepsilon)w_L^2\frac{\partial \rho_L}{\partial p} - \varepsilon w_G^2\frac{\partial \rho_G}{\partial p} + \Delta_1\frac{\partial \varepsilon}{\partial p} \tag{26}$$

Energy conservation for a single-phase flow is described by

$$\dot{q}\frac{U}{A} = \frac{\partial}{\partial z}\left(\rho w\left(h + \frac{w^2}{2} + gz\sin\beta\right)\right) \tag{27}$$

$$\dot{q} = \alpha(\vartheta_w - \vartheta) \tag{28}$$

In Eq. (27), enthalpy is a function of pressure and temperature, $h = h(p,\vartheta)$ and the partial differential of the enthalpy in the z direction can be expressed as

$$\frac{\partial h}{\partial z} = \frac{\partial h}{\partial p}\frac{\partial p}{\partial z} + \frac{\partial h}{\partial \vartheta}\frac{\partial \vartheta}{\partial z} \tag{29}$$

By differentiating Eq. (27) and substituting the expressions Eqs. (1) and (12), Eq. (27) can be written as

$$\alpha(\vartheta_w - \vartheta)\frac{U}{A} = w\left(1 + \rho\frac{\partial h}{\partial p}\right)\frac{\partial p}{\partial z} + \rho w\frac{\partial h}{\partial \vartheta}\frac{\partial \vartheta}{\partial z} + w\left|\frac{\partial p}{\partial z}\right|_R \tag{30}$$

and for a two-phase flow, it is given by

$$\dot{q}\frac{U}{A} = \frac{\partial}{\partial z}\big(\rho_L(1-\varepsilon)E_L w_L + \rho_G\varepsilon E_G w_G\big) \tag{31}$$

where $E_k = h_k + \frac{w_k^2}{2} + gz\sin\beta$ and the enthalpy in Eq. (31) depends on the pressure, $h_k = h_k(p)$. The partial differential of the enthalpies of steam and water phases in z direction can be formulated as

$$\frac{\partial h_k}{\partial z} = \frac{\partial h_k}{\partial p}\frac{\partial p}{\partial z} \tag{32}$$

The difference between h_G and h_L also depends on the pressure and can be expressed as

$$r(p) = h_G(p) - h_L(p) \tag{33}$$

The partial differential of r in the z direction can be given by

$$\frac{\partial r}{\partial z} = \frac{\partial r}{\partial p}\frac{\partial p}{\partial z} \tag{34}$$

By differentiating Eq. (31) and taking into account Eqs. (32)–(34), Eq. (31) can be written as

$$\frac{\dot{m}}{A}\left(F_1 + F_2\frac{\partial \varepsilon}{\partial \dot{x}}\right)\frac{\partial \dot{x}}{\partial z} + \frac{\dot{m}}{A}\frac{\partial r}{\partial p}\frac{\partial p}{\partial z}\dot{x} = F_3 \tag{35}$$

with

$$F_1 = r + \frac{3}{2}\big(-w_L^2 + w_G^2\big) \tag{36}$$

$$F_2 = \frac{A}{\dot{m}}\big(\rho_L w_L^3 - \rho_G w_G^3\big) \tag{37}$$

$$F_3 = F_4 + F_5\frac{\partial p}{\partial z} \tag{38}$$

$$F_4 = -\frac{\dot{m}}{A}\left(Y + \frac{A}{\dot{m}}\big(\rho_L w_L^3 - \rho_G w_G^3\big)\frac{\partial \varepsilon}{\partial p}\right) \tag{39}$$

$$Y = \frac{\partial h_L}{\partial p} + \frac{A}{\dot{m}}\left(-(1-\varepsilon)w_L^3\frac{\partial \rho_L}{\partial p} - \varepsilon w_G^3\frac{\partial \rho_G}{\partial p}\right) \tag{40}$$

$$F_5 = -\frac{\dot{m}}{A}g\sin\beta + \alpha(\vartheta_w - \vartheta)\frac{U}{A} \tag{41}$$

The tube wall energy balance can be written as

$$0 = \alpha_{hg}U_{hg}(\vartheta_{hg} - \vartheta_w) + \alpha_{wf}U_{wf}(\vartheta_{wf} - \vartheta_w) \tag{42}$$

This system of partial differential equations is solved numerically using the finite difference scheme (partial derivative approximation and spatial discretization with equidistant increments) to obtain the mass flow rate, pressure and temperature for the single-phase or steam quality for the two-phase flow. Additionally, the constitutive relationships are used to close the model [13–17]. In a single-phase flow in tubes, the friction pressure gradient is determined as follows:

$$\left|\frac{\Delta p}{\Delta z}\right|_R = \frac{\xi}{2d}\rho w^2 \tag{43}$$

where, the Haaland correlation [13] is used to calculate the friction factor ξ:

$$\xi = \left[3.24\left(\log\left(\frac{6.9}{Re} + \left(\frac{\varepsilon_r/d_i}{3.7}\right)^{1.11}\right)\right)^2\right]^{-1} \tag{44}$$

The two-phase friction pressure gradient is calculated using the equation:

$$\left|\frac{\Delta p}{\Delta z}\right|_{\text{two-phase}} = \left|\frac{\Delta p}{\Delta z}\right|_{\text{single-phase}}\Phi_{\text{Lo}}^2 \tag{45}$$

where $|\frac{\Delta p}{\Delta z}|_{\text{single-phase}}$ is the liquid single-phase friction pressure gradient based on the total mass flow rate of the two-phase mixture and Φ_{Lo}^2 is the corresponding two-phase multiplier as determined with the Friedel correlations [16,17]:

$$\Phi_{\text{Lo}}^2 = A + B_u \tag{46}$$

for upward flow and

$$\Phi_{\text{Lo}}^2 = A + B_d \tag{47}$$

for downward flow.

The terms A, B_u, and B_d in Eqs. (46) and (47) are given by:

$$A = (1-\dot{x})^2 + \dot{x}^2\left(\frac{\rho_L \xi_G}{\rho_G \xi_L}\right) \tag{48}$$

$$B_u = 3,43\dot{x}^{0.69}(1-\dot{x})^{0,24} B_{u1} \tag{49}$$

$$B_{u1} = \Lambda_1 Fr_L^{-0,047} We_L^{-0,0334} \tag{50}$$

with

$$\Lambda_1 = \left(\frac{\rho_L}{\rho_G}\right)^{0.8}\left(\frac{\eta_L}{\eta_G}\right)^{0.22}\left(1-\frac{\eta_L}{\eta_G}\right)^{0.899} \tag{51}$$

$$B_d = 38.5\dot{x}^{0,76}(1-\dot{x})^{0,314} B_{d1} \tag{52}$$

$$B_{d1} = \Lambda_2 Fr_L^{-0,0001} We_L^{-0,037} \tag{53}$$

$$\Lambda_2 = \left(\frac{\rho_L}{\rho_G}\right)^{0.86}\left(\frac{\eta_L}{\eta_G}\right)^{0.73}\left(1-\frac{\eta_L}{\eta_G}\right)^{6.84} \tag{54}$$

The Froude number in Eq. (53) is evaluated from

$$Fr_L = \frac{\dot{m}^2}{g d_i \rho_L^2} \tag{55}$$

The calculation of the Weber number in Eq. (53) is done using the equation:

$$We_k = \frac{\dot{m}^2 d_i}{\rho_L \sigma} \tag{56}$$

According to Friedel's correlations, the friction factor is given by

$$\xi_k = \frac{64}{Re_k} \tag{57}$$

for $Re_k \leqslant 1055$ and

$$\xi_k = \left[0.86859 \ln \frac{Re_k}{1.964 \ln Re_k - 3.8215}\right]^{-2} \tag{58}$$

for $Re_k > 1055$.

An in-line configuration was chosen to represent the tube arrangement in the tube banks. Thus, the friction pressure drop on the exhaust gas side can be evaluated by [14,15,17]:

$$\Delta p = \xi N_w \frac{\rho w_e^2}{2} \tag{59}$$

where w_e is the maximum gas flow velocity that will occur through the minimum frontal area. This velocity can be written as follows:

$$w_e = \frac{a}{(a-1)} w \tag{60}$$

with $a = \frac{s_1}{d}$, s_1 the transversal pitch and w the free stream gas velocity.

N_w is the number of transverse rows in the gas flow direction.

The friction factor ξ is given by

$$\xi = \xi_1 + \xi_t\left(1 - e^{(-\frac{Re+1000}{2000})}\right) \tag{61}$$

where Re is given by

$$Re = \frac{w_e d_o \rho}{\eta} \tag{62}$$

ξ_l is the laminar friction factor, calculated from

$$\xi_1 = \frac{280\pi(((s_2/d_o)^{0.5} - 0.6)^2 + 0.75)}{Re(4 s_1 s_2/d_o^2 - \pi)(s_1/d_o)^{1.6}} \tag{63}$$

and s_2 is the longitudinal pitch of the in-line configuration tube banks array.

The turbulent friction factor ξ_t is written as

$$\xi_t = \frac{1}{Re^{0.1 S_2/S1}}(J_1 + 0.03 J_2) \tag{64}$$

with

$$J_1 = 10^{0.47(s_2/s_1 - 1.5)}(0.22 + J_{1,1}) \tag{65}$$

$$J_{1,1} = 1.2\left(1 - 0.94\frac{d_o}{s_2}\right)^{0.6} \Big/ \left(\frac{s_1}{d_o} - 0.85\right)^{1.3} \tag{66}$$

$$J_2 = \left(\frac{s_1}{d_o} - 1\right)\left(\frac{s_2}{d_o} - 1\right) \tag{67}$$

The single-phase heat transfer coefficient on the working fluid side is given by

$$\alpha_{wf} = \frac{Nu_0 \lambda wf}{d_i} \tag{68}$$

where Nu_0 is the Nusselt number, which can be written as

$$Nu_0 = 0.0214\left(Re^{0.8} - 100\right)Pr^{0.4} Y_d \tag{69}$$

with $Y_d = 1 + (d_i/L_{\text{tube}})^{2/3}$ for $0.5 < Pr < 1.5$ and $10^4 < Re < 510^6$ and

$$Nu_0 = 0.012\left(Re^{0.87} - 280\right)Pr^{0.4} Y_d \tag{70}$$

for $1.5 \leqslant Pr < 500$ and $3000 < Re < 10^6$.

The two-phase flow heat transfer coefficient is calculated using [18]:

$$\alpha_{wf} = \frac{0.06136}{(1 - (\vartheta_{\text{sat}}/378.64)^{0.0025})^{0.73}} \dot{q}^{0.673} \tag{71}$$

where ϑ_{sat} and $\dot{q}$ are expressed in °C and W·m^{-2}, respectively.

The Nusselt number on the exhaust gas side is found from

$$Nu = f_A Nu_0 \tag{72}$$

where f_A is the arrangement factor and determined as follows:

$$f_A = 1 + \frac{0.7}{\psi^{0.5}} \frac{s_2/s_1 - 0.3}{(s_2/s_1 + 0.7)^2} \tag{73}$$

with ψ as the void ratio, which can be formulated as

$$\Psi = 1 - \frac{\pi}{4 s_1/d_o} \tag{74}$$

for $s_2/d_o > 1$ and

$$\Psi = 1 - \frac{\pi}{4 s_1 s_2/d_o^2} \tag{75}$$

for $s_2/d_o < 1$.

The Nusselt number Nu_0 is described by

$$Nu_0 = 0.3 + \sqrt{Nu_1^2 + Nu_t^2} \tag{76}$$

where the laminar Nusselt number is given by

$$Nu_1 = 0.664 Re_\psi^{1/2} Pr^{1/3} \tag{77}$$

and the turbulent Nusselt number is expressed as

$$Nu_t = \frac{0.037 Re_\psi^{0.8} Pr}{1 + 2.443 Re_\psi^{-0.1}(Pr^{2/3} - 1)} \tag{78}$$

In Eq. (78), the Reynolds number is calculated using the equation:

$$Re_\psi = \frac{wL\rho}{\psi\eta} \tag{79}$$

Finally, the heat transfer coefficient on the exhaust gas side can be written as follows:

$$\alpha_{\text{hg}} = \frac{\lambda_{\text{hg}} Nu}{L} \tag{80}$$

with $L = \frac{\pi}{2} d_o$.

When external finned tube banks are used [13,14], their effect on the heat transfer coefficient calculation is taken into account by means of the following ratio:

$$\frac{A_t}{A_{\text{wf}}} = 1 + 2\frac{L_f(L_f + d_o + t_f) + t_f^2/4}{d_o s_f} \tag{81}$$

where A_t, A_{wf}, L_f, s_f and t_f are the total surface area of a finned tube, base surface area of the tube without fins, fin length, fin pitch and fin thickness, respectively. The fins are assumed to have a circular shape.

4. Numerical results and discussion

The solutions depend on the specific boundary conditions for the models investigated. Mass flow rate and temperature on the working fluid side were assumed to be constant at the inlet of both systems. For all models, high and intermediate pressure levels on the working fluid side were chosen for systems 1 and 2, respectively, as shown in Tables 1 and 2.

Table 1
Working fluid data for model 1

	Mass flow rate kg·s^{-1} inlet	Pressure bar outlet	Temperature °C inlet
System 1	13	100	100
System 2	14.5	20	100

Table 2
Working fluid data for model 2

	Mass flow rate kg·s^{-1} inlet	Pressure bar outlet	Temperature °C inlet
System 1	23	100	180
System 2	7.8	20	100

Water and steam properties were computer calculated using the water-steam relations in [19].

The exhaust gas parameters were taken at the outlet conditions of the gas turbine. This outlet was characterized by the exhaust gas state, i.e., mass flow rate, temperature and pressure. The values of 220 kg·s^{-1}, 1 bar and 560 °C were chosen for the mass flow rate, pressure and temperature on the exhaust gas side, respectively [4]. To calculate the thermodynamic state of the exhaust gas, a FORTRAN program was developed from the polynomial functions in [20], which depend on exhaust gas temperature. This program permits the determination of exhaust gas enthalpy, specific heat, thermal conductivity, dynamic viscosity, and Prandtl number for dry air at 1 bar. Specific volume was calculated using the ideal gas relationship.

4.1. Effect of tube length

To investigate the effect of tube length on the outlet exhaust gas and working fluid parameters, the tube diameter was kept constant with values of 0.0316 and 0.038 mm for

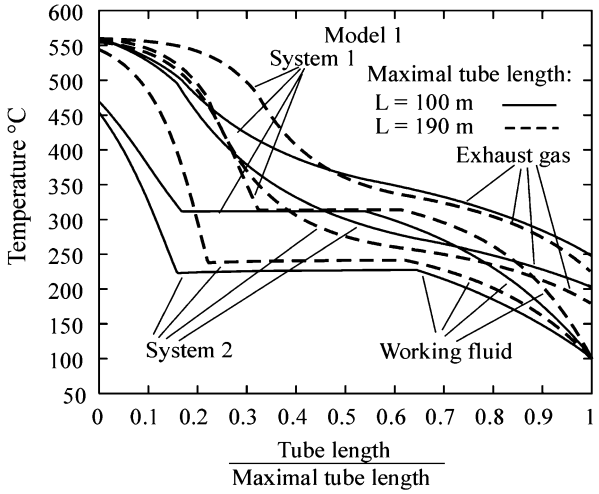

Fig. 3. Temperature versus tube length ratio.

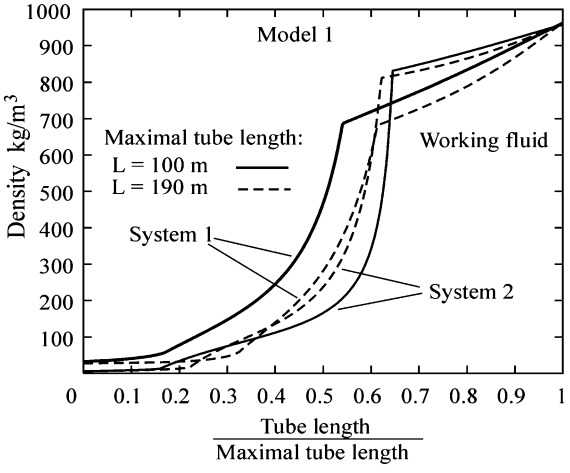

Fig. 4. Density versus tube length ratio.

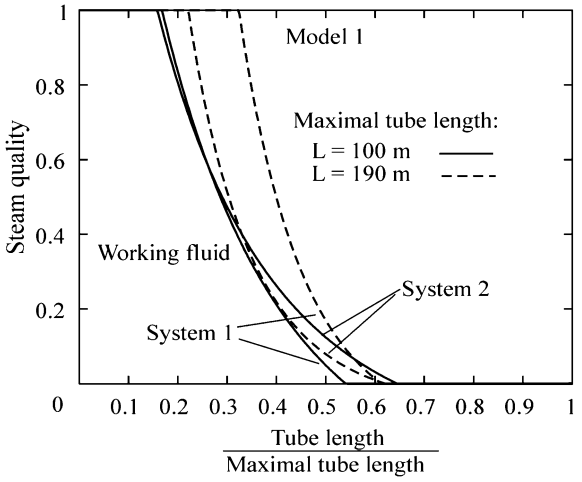

Fig. 5. Steam quality versus tube length ratio.

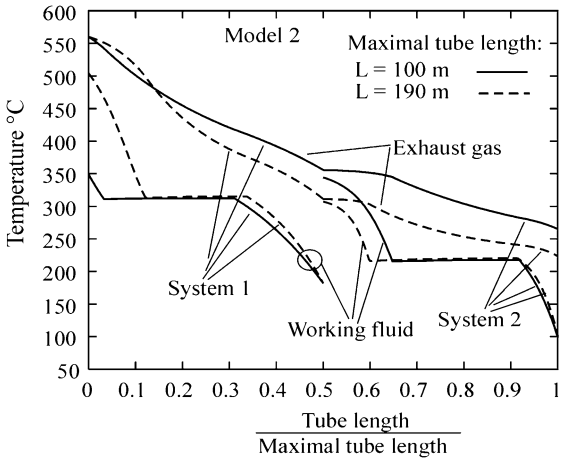

Fig. 6. Temperature versus tube length ratio.

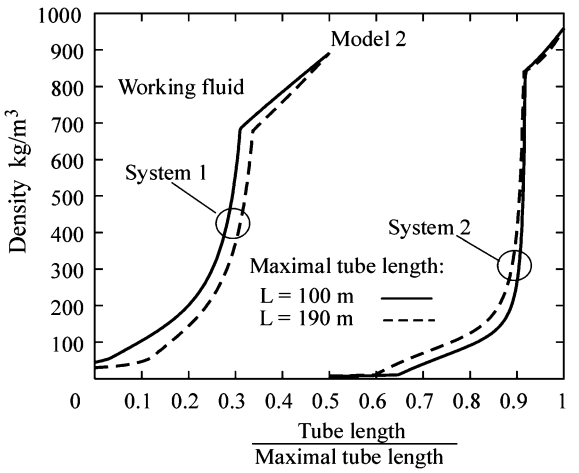

Fig. 7. Density versus tube length ratio.

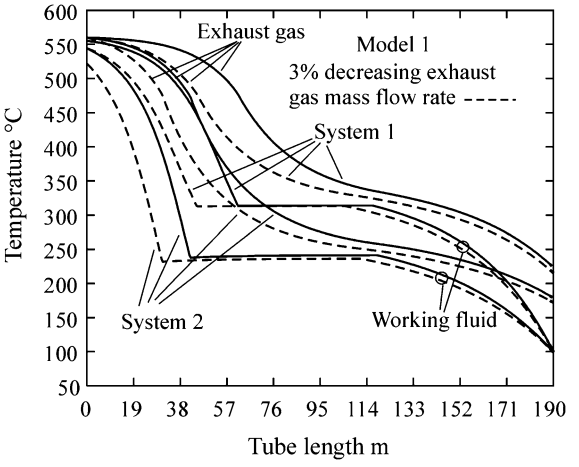

Fig. 8. Temperature versus tube length.

the inner and outer diameters, respectively. For model 1, Fig. 3 shows decreasing outlet exhaust gas temperature with increasing tube length ratio. In this case, a 90% increase in the tube length from 100 m leads to a 10.8% reduction in average outlet exhaust gas temperature. This has an impact on the boiling point of the working fluid. The corresponding curves in the density and steam quality as a function of the tube length ratio are shown in Figs. 4 and 5 for the tube side of both systems.

For model 2, Figs. 6 and 7 show the temperature and density as a function of the tube length ratio. From Fig. 6, it can be observed that the tube length plays an important role in reducing the outlet exhaust gas temperature, which corresponds to a decrease of 15.83% from 265.21 °C. Moreover, the working fluid parameters depend on the tube length ratio, as shown in Figs. 6 and 7.

4.2. Effect of decreasing exhaust gas mass flow rate

In order to examine the effect of reducing the exhaust gas mass flow rate on the working fluid parameters, the exhaust gas temperature was kept constant and the exhaust gas mass flow rate was reduced by 3% from 220 $kg \cdot s^{-1}$ for models 1 and 2. The diminution of the exhaust gas mass flow rate in model 1 leads to a decrease in outlet working fluid temperature of 2% from 555.2 °C and 4.1% from 544.11 °C for systems 1 and 2, respectively. Moreover, the average outlet exhaust gas temperature decreases 3.6% from 201 °C, as shown in Fig. 8. In addition, from this figure, one can observe the displacement of the boiling end point of the working fluid to the tube outlet for both systems.

For model 2, Fig. 9 shows the working fluid temperature reduction of 2.8% from 504.3 °C for system 1 and 7.2% from 307.1 °C for system 2 at the tube outlets. This is due to a decreasing exhaust gas mass flow rate. The exhaust gas temperatures for systems 1 and 2 are reduced 1.4% from 311.3 °C and 2.5% from 223.2 °C, respectively. Additionally, for both systems, the outlet exhaust gas temperature shows a tendency to decrease with reduction of the exhaust gas mass flow rate.

4.3. Effect of decreasing exhaust gas temperature

The reduction in the exhaust gas temperature has an influence on the working fluid parameters for all studied models.

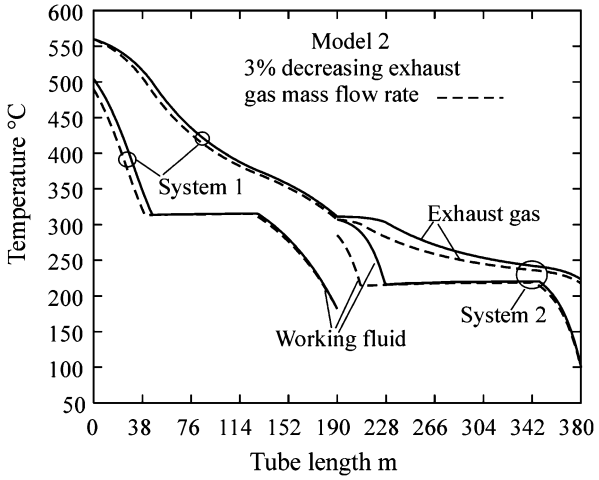

Fig. 9. Temperature versus tube length.

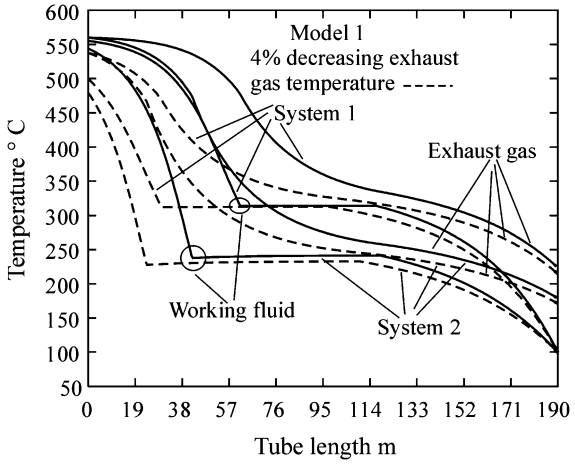

Fig. 10. Temperature versus tube length.

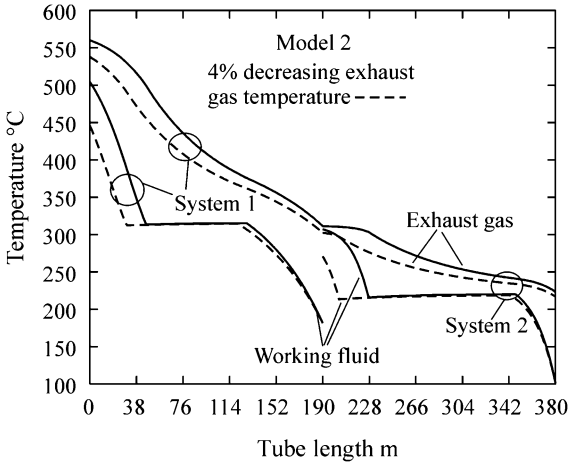

Fig. 11. Temperature versus tube length.

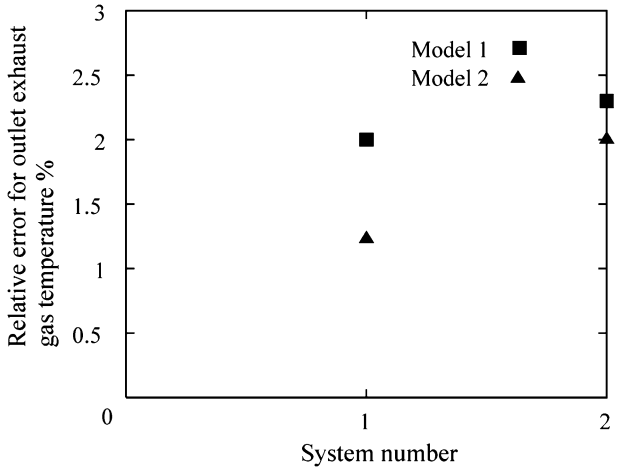

Fig. 12. Relative error for outlet exhaust gas temperature versus system number.

Fig. 10 shows the temperature as a function of tube length for model 1. Here, it can be observed that there is a decrease in working fluid temperature at the tube outlet of 10% from 555.2 °C and 11.8% from 544.1 °C for systems 1 and 2, respectively. The average outlet exhaust gas temperature shows a decrease of 4.1% from 200.9 °C.

For model 2, the 4% reduction of exhaust gas temperature leads to an 11.5% decrease of outlet working fluid temperature from 504.3 °C for system 1 and 12% from 307.1 °C for system 2 as shown in Fig. 11.

4.4. Model comparison

From the previous investigations on the models 1 and 2, Figs. 3–11, it can be summarized that a variation in one or more of the working fluid parameters in either of the systems of model 1 has no effect on the other system. However, in model 2, both reduction and increase in the working fluid parameters in system 1 have a strong effect on system 2, which depends on the heat transfer between the exhaust gas and system 1. Moreover, to valid the developed models, the outlet exhaust gas temperatures numerically determined were compared to them obtained using the calculation approach for flow across banks of finned tubes described in [14]. The tube length of 190 m and the data of Tables 1 and 2 were considered keeping the same conditions for the exhaust gas parameters. The outlet exhaust gas temperatures from the calculation approach for flow across banks of finned tubes [14] and present work showed good agreement with relative errors of less than 2.5% for both models, as shown in Fig. 12.

5. Conclusion

For this study, two different models of dual-pressure finned tube banks were developed and numerically investigated for the effect of the exhaust gas parameters and tube length. The relevant physical phenomena were accounted for by means of a non-linear approach and the difference between water and steam velocities in finned tubes. The results obtained show that the variation of the exhaust gas parameters, mainly temperature and mass flow rate, strongly and differently affects the static behavior of the models. Fur-

thermore, the results demonstrate a tendency for the outlet exhaust gas temperature to decrease with increasing tube length for improved waste heat utilization.

Acknowledgement

The authors are grateful to the Foundation of the University of Quebec in Abitibi-Temiscamingue (FUQAT).

References

[1] G. Heyen, B. Kalitventzeff, A comparison of advanced thermal cycles suitable for upgrading existing power plant, Appl. Thermal Engrg. 19 (1999) 227–237.
[2] J.S.H. Najjar, Efficient use of energy by utilising gas turbine combined systems, Appl. Thermal Engrg. 21 (2001) 407–438.
[3] B. Gericke, Integrated waste heat utilisation in pipeline compressor stations. Part 1: Gas turbines for compressor stations, VGB Power Tech. 2 (2002) 64–69.
[4] R. Kehlhofer, R. Bachmann, H. Nielsen, J. Warner, Combined-Cycle Gas and Steam Turbine Power Plants, Pennwell Publishing Company, Tulsa, OK, 1999.
[5] J.H. Horlock, Advanced Gas Turbine Cycles, Elsevier, Amsterdam, 2003.
[6] A. Franco, A. Russo, Combined cycle plant efficient increase based on the optimization of the heat recovery steam generator operating parameters, Internat. J. Thermal Sci. 41 (2002) 843–859.
[7] M.S. Mon, U. Gross, Numerical study of fin-spacing effects in annular-finned tube heat exchangers, Internat. J. Heat Mass Transfer 47 (2004) 1953–1964.
[8] A.S. Wilson, M.K. Bassiouny, Modeling of heat transfer for flow across tube banks, Chem. Engrg. Processing 39 (2000) 1–14.
[9] K. Bilen, U. Akyol, S. Yapici, Thermal performance analysis of a tube finned surface, Internat. J. Energy Res. 26 (2002) 321–333.
[10] Z. Rouhani, Modified correlations for void fraction and two-phase pressure drop, AE-RTV-841, 1969.
[11] B. Chexall, et al., Void Fraction Technology for Design and Analysis, EPRI Electric Power Research Institute, 1997.
[12] S. Kakaç, A.E. Bergles, F. Mayinger, Heat Exchangers, Thermal-Hydraulic Fundamentals and Design, Advanced Study Institute Book, Hemisphere Publishing Corporation, Springer, Berlin, Heidelberg, New York, Tokyo, 1980.
[13] F.M. White, Fluid Mechanics, fifth ed., McGraw-Hill, New York, 2003.
[14] F.P. Incropera, D.P. DeWitt, Fundamentals of Heat and Mass Transfer, fourth ed., Wiley, New York, 2002.
[15] J.P. Holman, Heat Transfer, eighth ed., McGraw-Hill, New York, 1997.
[16] L. Friedel, Pressure drop during gas/vapour liquid flow in pipes, Internat. Chem. Engrg. 20 (1980) 352.
[17] Ingenieure, Verein Deutscher, VDI-Wäarmeatlas, Berechnungsblätter für den Wärmeübergang, 8. Auflage, VDI-Verlag, Düsseldorf, 1997.
[18] F. Brandt, Wärmeübertragung in Dampferzeugern und Wärmeaustauschern, Band 1, Fachverband Dampfkessel, Behälter und Rohrleitungsbau, Deutschland, 1980.
[19] E. Schmidt, Properties of Water and Steam in SI-Units, Springer, Berlin, 1989.
[20] F. Brandt, Wärmeübertragung in Dampferzeugern und Wärmeaustauschern, Band 2, Fachverband Dampfkessel, Behälter und Rohrleitungsbau, Deutschland, 1985.